

EVALUATION OF THE SEISMIC PERFORMANCE OF COMBINED FRAME-WALL-FOUNDATION STRUCTURAL SYSTEMS THROUGH CENTRIFUGE TESTING

**Barbara CHANG, Prishati RAYCHOWDHURY, Tara HUTCHINSON¹, Jeremy THOMAS²,
Sivapalan GAJAN³, Bruce KUTTER⁴**

ABSTRACT

Numerous existing low-ductility reinforced-concrete (R/C) buildings are commonly retrofit with an additional shear wall to withstand seismically generated lateral forces. For the retrofit structure, the foundation compliance and its potential yielding under large earthquake input is rarely accounted for, resulting in a system whose seismic response is poorly understood. To investigate the seismic performance of combined frame-wall-foundation systems, an idealized planar R/C frame with an attached shear wall and shallow foundations, resting on dense dry sand, was designed and in a first attempt to incorporate structural nonlinearity into a centrifuge model, beam nonlinearity is accounted for by using replaceable ductile fuses at the beam-ends. Modeled after the idealized structure, two 1/20th scale steel models were tested in the centrifuge at the University of California, Davis. Models were loaded using inertial-based displacement-controlled reversed cyclic demands and dynamic base shaking. Response of the models is evaluated in terms of global lateral force-displacement, local footing (moment-rotation, shear-sliding, axial-settlement), and local beam-column moment-rotation histories. Lateral force-displacement response shows that these frame-wall systems have highly asymmetric hysteretic loops due to the asymmetry of the lateral force resisting system. Additionally, it is observed that energy is dissipated through the modes of rocking, sliding, and settlement of the footings for both foundation-structural models tested. Evaluation of the energy dissipated at the footing-soil interface indicates that at low drift ratios, the footings can account for more than 90% of the total system dissipated energy. Despite increasing drift demand on the structure, the energy dissipated by the footings does not drop below 65% of the total.

Keywords: seismic soil-structure interaction, energy dissipation, centrifuge tests, shallow foundations

INTRODUCTION

The seismic performance of dual frame-wall systems resting on shallow foundations is influenced by the flexibility of the underlying foundation as well as that of the structural components (for example, the beam-column joints). However, conventional design practice generally does not account for the flexibility of the underlying foundation; nor does it consider the design of the frame and wall as a system. Under large seismic excitations, mobilization of the bearing capacity below the wall footing may occur, resulting in nonlinear soil interface behavior that will dissipate energy. These large demands at the foundation level must be controlled to ensure stability against bearing failure and

¹ Graduate Student (BJC and PRC) and Associate Professor (TCH), respectively, Department of Structural Engineering, University of California, San Diego, La Jolla, CA 92093.

² Staff Engineer, G2 Consulting Group, LLC, 1866 Woodslee Street, Troy, Michigan

³ Assistant Professor, Department of Civil Engineering, North Dakota State University, Fargo, ND 58105.

⁴ Professor, Department of Civil and Environmental Engineering, University of California, Davis, Davis, CA, 95616.

minimize settlement. Under these conditions, if the energy dissipative qualities of the wall foundation are harnessed, then superstructure demands can be reduced significantly. However, to account for this dissipation of energy in performance-based earthquake engineering, several issues must be considered. First, the rocking motion of the wall can result in undesirable and excessive cyclic and permanent settlement at the footing. Second, the nature of the redistribution of demands within the foundation-structural system must be considered, particularly as the footing yields. The second issue is of particular importance for combined structural systems, where rocking of the foundation below one system may induce large demands at the superstructure interface due to their difference in stiffness. For example, in a wall-frame system, the more flexible moment frame will have a lower stiffness than the very rigid shear wall.

Studies of the behavior of rigid elements under rocking motion stem from the early work of Housner (1963). Subsequent experimental studies have substantiated the beneficial energy dissipating features of rocking foundation systems (e.g. Barlett, 1976; Wiessing, 1979; Negro et al., 1998). Recent work at the University of California, Davis, (UC Davis), has considered an idealized shallow foundation (strip footing) supporting a shear wall structure subjected to a variety of loading conditions, including reversed cyclic rocking motion and base excitation. These experiments, conducted by Rosebrock and Kutter (2001) and Gajan et al. (2003), denoted herein as the KRR and SSG series, respectively, have examined a range of footing sizes, static vertical factors of safety, and both clay and sand soil types. Shallow foundation models were subjected to static and dynamic pushes: pure compression, lateral displacement cyclic loading, and base excitation. Analysis and subsequent analytical modeling of KRR and SSG experimental data (Gajan et al., 2005; Harden 2003) demonstrated that significant energy is dissipated at the soil-foundation interface.

Experiments described in this paper extend the foundation-wall models of the KRR and SSG centrifuge experiments to consider more complex foundation-structural systems. These models are intended to idealize portions of real building structures. The selected portion involves an idealized reinforced concrete (R/C) two-story, two-bay moderate ductility frame attached to a shear wall, which is supported on shallow isolated square and strip footings. Two scale models of these systems were then constructed and tested on the geotechnical centrifuge at 20g's (Chang et al., 2006a and 2006b). In the following presentation of the experimental program and results, all units are presented at prototype scale, unless noted otherwise.

EXPERIMENTAL PROGRAM

Geotechnical Centrifuge at UC Davis

The frame-wall-foundation model structure was designed to fit within a 1.76×0.9 meter rigid soil container mountable on the UC Davis centrifuge. For these tests, the soil container was spun to create a gravitational field of 20g's applied to the model. According to centrifuge scaling laws, a specimen subjected to 20g's is dimensionally twenty times larger than its size at 1-g. Most importantly, stresses scale 1:1 from model to prototype. This direct 1:1 scaling of stress is especially valuable for geotechnical engineering because soil properties are very sensitive to confining stress. However, the principles of centrifuge modeling can also be easily applied to structures, and it is valuable for problems that involve nonlinear soil-structure interaction. The centrifuge allows modeling of prototype soil stresses and, thus, captures the strength and deformation characteristics of the soil. Additional description of the centrifuge and information regarding governing scaling laws may be found in Kutter (1997).

Prototype Frame-Wall-Foundation Design

A hypothetical prototype consisting of a two-story, two-bay, planar R/C frame with an attached shear wall was designed using recent seismic design guidelines (FEMA 356, 2000). Design gravity loads were selected assuming a surface load of 1.3 kPa acting over 4.6 meters tributary width. Prototype frame dimensions of 9.53×7.62 meters (height \times width) and a shear wall of 9.53×2.54 meters were selected. Member stiffness was tuned to achieve a target fundamental (flexible base) period of

approximately $T_n=0.5$ seconds. Shallow footings were designed to support the structure, with a strip footing beneath the shear wall and square footings beneath individual columns. The footings were not connected. Each footing was designed with static vertical factors of safety well above typical design (governing $FS_v=5.4$, under service load conditions). The R/C frame was designed for ductile behavior using ACI 318-02 (2002) recommendations. Confined concrete beams were designed using moment-curvature relations developed with Mander's confinement model (Mander et al., 1988).

To evaluate the response of the designed frame-wall-foundation system, an OpenSEES (2006) model was constructed and pushover analyses conducted. Figure 1 shows a schematic of the prototype and numerical model constructed. Flexibility of the underlying soil foundation was modeled using nonlinear spring elements, which incorporate radiation damping effects and allow the structure to rock, slide, and/or settle in the soil. Constitutive soil parameters for the nonlinear soil-foundation springs (bearing capacity, stiffness, etc.) were derived from KRR and SSG test results. Columns were modeled using nonlinear beam-column elements. Beams were designed to yield with design level seismic forces through forced hinges at the ends of typical beam-column joints. The plastic hinge behavior of the beams was later mimicked by custom-designed steel fuses in the centrifuge model.

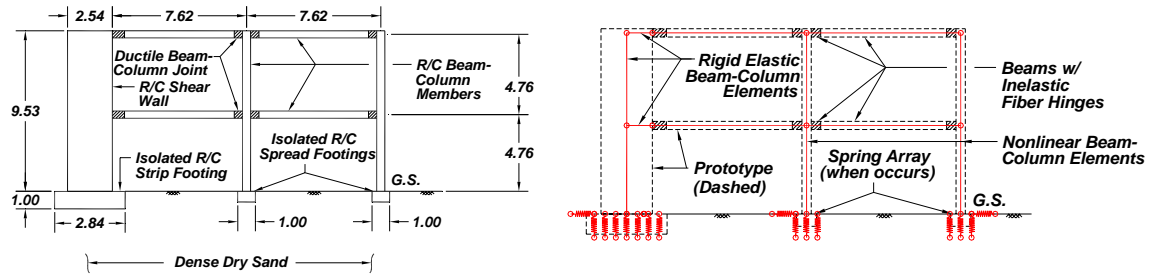


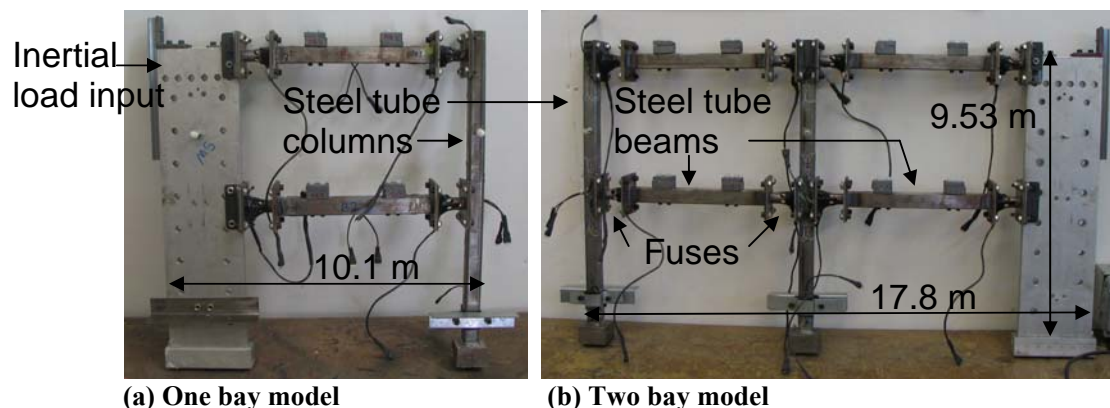
Figure 1. Prototype and numerical model of wall-frame-foundation system under study (units: meters).

The idealized prototype building was reduced to 20g model-scale, and frame-wall structural and foundation elements were fabricated from steel and aluminum. Due to the workability of steel, the frame elements (beams and columns) were constructed from steel tubing (Figure 2). The existing aluminum shear wall and strip footing from previous KRR and SSG test series were adapted for these experiments. Lead mass blocks simulated the remaining dead load of the structure. Moment transferring bolted connections attached all beam-column (fuse) and frame-to-shear-wall (fuse) connections. The modularity of the connections and pieces enabled the model to be assembled into the original two-story two-bay configuration and also a modified two-story one-bay configuration (Figure 2a and b). The modified one bay model was tested first, as its instrumentation was simpler and thus easier to post-process. After scaling to 20g's, overall dimensions of the one bay model were 0.51×0.51 meters; dimensions of the two bay were 0.51×0.89 meters. Each model was tested at a different station location within the soil box. Eigenvalue analysis of the OpenSEES model of the centrifuge model indicate the natural period of the system (combined frame-wall-foundation structure resting on a flexible soil foundation) was 0.38 seconds for the one bay model and 0.33 seconds for the two bay model.

Instrumentation

Instrumentation for the structure was arranged to capture data from: local load distributions of shear, moment, and axial forces; global and local displacements; and lateral, vertical, and out-of-plane accelerations. The structure was slightly embedded about 0.1 meter in a 4 meter thick layer of dry dense Nevada sand, which was instrumented with embedded accelerometers. Strain gages were attached to elastic regions of the beams and columns for recording the moment at specific locations. Fuses were instrumented with high-elongation ($200,000 \mu\epsilon$ or 20% capacity) strain gages in a full-bridge configuration to directly measure changes in strain. Fuse moments were then based on calibration tests conducted at 1g. Vertical linear potentiometers were placed at the ends of each footing and used to calculate settlements and rotations. Laterally placed linear potentiometers measured

sliding of individual footings and horizontal movement of the shear wall and columns. The one bay structure had approximately forty instruments, while the two bay had approximately sixty instruments.



(a) One bay model

(b) Two bay model

Figure 2. Assembled centrifuge models (prototype units).

Test Series

While at 20g's both models were tested under a series of slow cyclic static lateral pushes and tapered cosine dynamic base input shakes (Table 1). In addition, the two bay model was excited by a 1989 Loma Prieta earthquake motion recorded in Santa Cruz, California (test D9). Using the same soil box and different stations, the one bay model was tested first and removed; then the two bay model was placed on the other side of the soil box and tested. Static pushes were input as inertial-based loading at the upper floor level through a hydraulic actuator (Figure 2a); dynamic shakes were input at the base of the soil layer through a shake table mounted beneath the soil box. All loading was applied in plane with the frame-wall-foundation models.

Table 1. Testing chronology for the one bay and two bay models.

One Bay Tests			Two Bay Tests		
Test	Date	Abs drift (%)	Test	Date	Abs drift (%)
HSC 1	Dec 10	0.01	HSC 9	Dec 20	0.02
HSC 2	Dec 10	0.03	HSC 10	Dec 20	0.05
D 1 (0.09 g)	Dec 15	0.01	HSC 11	Dec 20	0.06
D 2 (0.20 g)	Dec 15	0.03	D 5 (0.08 g)	Dec 21	0.06
D 3 (0.65 g)	Dec 15	1.73	D 6 (0.14 g)	Dec 21	0.07
D 4 (0.93 g)	Dec 15	3.54	D 7 (0.65 g)	Dec 21	1.11
HSC 3	Dec 16	3.54	D 8 (0.96 g)	Dec 21	1.73
HSC 4	Dec 16	3.56	D 9 (0.85 g)	Dec 21	1.79
HSC 5	Dec 16	3.59	HSC 12	Dec 21	1.79
HSC 6	Dec 16	3.63	HSC 13	Dec 21	1.80
HSC 7	Dec 16	3.61	HSC 14	Dec 21	1.85
HSC 8	Dec 16	3.73	HSC 15	Dec 21	1.92
Abs drift = Total horizontal disp/Height Results from shaded tests are shown herein.			HSC 16	Dec 22	2.16
			HSC 17	Dec 22	2.19

EXPERIMENTAL RESULTS

Data Analysis

Instrument signals were recorded before spin up of the centrifuge, during testing, and after spin down of the centrifuge arm. To correctly post-process the data, use of recorded data from the instruments at 1g (before spin up of the centrifuge) was necessary. Initial voltages at 1g are used for zeroing data from the actuator load cell, beam and column moments, and fuse moments for each spin up. Zero

voltages for displacements were taken from 20g data from either HSC1 for the one bay or HSC9 for the two bay; subsequent displacements are cumulative. Response of the footings is then calculated from the internal forces of the beams and columns at static instances in time. For both the one bay and two bay models, a free-body diagram of each model was drawn, and sections cut at the location of each moment-capturing instrument. Values for moment, shear, and axial forces for the cut sections are calculated from the resulting static equations of equilibrium (Chang et al., 2006a).

Force-Displacement Response

Inspection of the global force and cumulative absolute displacement of both the one bay and two bay models reveal that hysteretic energy dissipation is occurring for both static and dynamic loading. Non-symmetrical stiffness of the structures is observed in the global force versus displacement response of the models (Figure 3). This behavior is more apparent for the one bay model (Figures 3a and b) than the two bay (Figures 3c and d). Tests D3 and HSC4 show the fluctuating values in stiffness as the structure is pushed in the direction of the column (negative displacement) and then pulled in the direction of the wall (positive displacement). Note that the model is sliding (permanently drifting) towards the weak (column) side; this behavior is particularly observed in test D3 (Figure 3a). Test D7 and HSC15 exhibit similar behavior – although after initial displacement in test HSC 15, the structure behaves in a more symmetric manner by rocking about the middle square footing (Figure 3d). In Figure 3, seismic coefficient “C” is defined as shear force divided by weight of the structure.

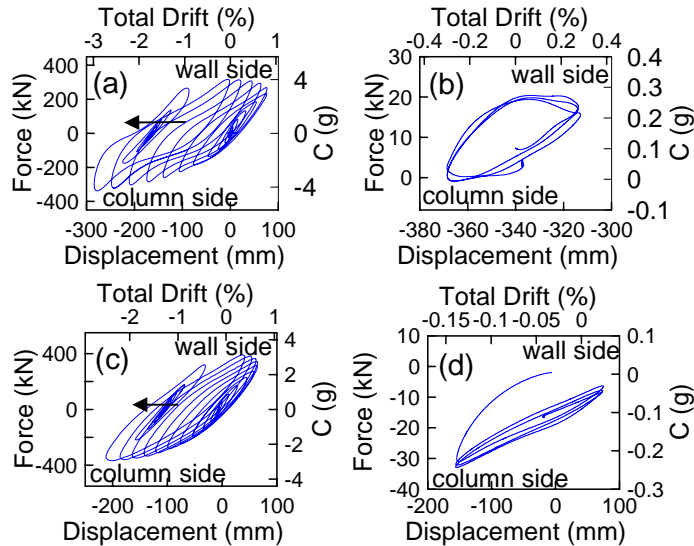


Figure 3. Force versus displacement response of models:
(a) one bay test D3, (b) one bay test HSC4, (c) two bay test D7, and (d) two bay test HSC15.

the one bay continues, the rotations for these two footings become increasingly divergent. Consequently, although the model moves as a whole towards the column side, the one bay strip footing rotates cumulatively in the positive direction, while the one bay square footing rotates cumulatively in the negative direction (Figure 4a). In contrast, the two bay footings tend to rotate in the same direction (Figure 4b). As the sequence of two bay tests continues, the strip footing and both square footings rotate further in the positive direction. This contrasting footing rotation may be from the differing geometries of the two models; the two bay model is more symmetrical and less slender than the one bay model. This symmetry may be the reason for the similar behavior among the two bay footings. Cumulative soil gapping during previous loading of the square footing and/or densification at the strip footing may also explain the divergent behavior of the one bay footings.

Graphical depiction of the observed deformed shape of the models during testing are shown for the one bay in test D3 and the two bay in test D7 (Figure 4). These drawings are shown with exaggerated rotations and displacements of the footings, beams, and columns. Of particular note, the trend of the footing rotation for the one bay model differs from that of the two bay model. The one bay strip footing is rotating in the opposite direction as the square footing due to the cumulating plastic rotations at the beam column joints and the outward sliding of the column footing due to potential gap development from previous loading. As the testing sequence of

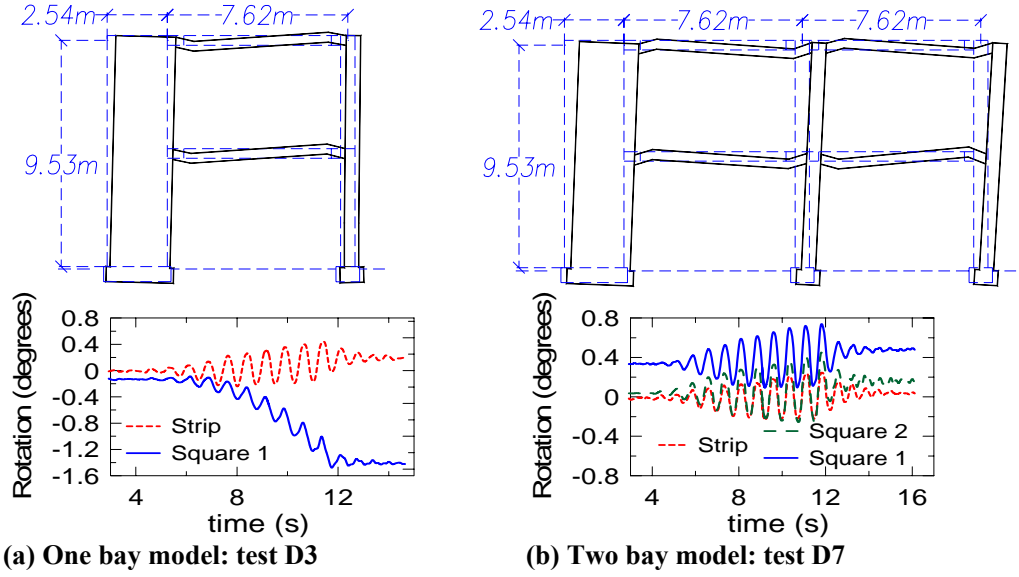


Figure 4. Deformed shape and footing rotation time history. Initial position of structure is shown dashed.

Fuse Response

Moment-rotation behavior of the fuses is calculated from calibration experiments conducted at 1g. Calibration of these ductile fuses consisted of testing four fuses under slow reversed cyclic loading in a cantilever configuration, with three cycles applied at each of 0.5, 0.75, 1.0, 2.0, 3.0, and 4.0 times Δy , where Δy is the estimated yield displacement. A Romberg-Osgood model was then fit to the recorded moment-rotation response. The average values of the parameters from the Romberg-Osgood regression are then used to calculate an analytical moment from the recorded strain data from the centrifuge experiments. From these tests, a yield moment of 200 kN m and a yield rotation of 0.04° was estimated.

Comparison of the energy dissipated by the fuses in the bottom and top floors demonstrates that the bottom fuses as a whole dissipate more energy than the top floor fuses due to the larger local rotations imposed at the lower floors, as may be expected. Sample data from test HSC16 is shown in Figure 5, where the solid line indicates the ratio of the summation of the energy dissipated by the top floor fuses divided by the total energy dissipated by all fuses. The dashed line indicates the ratio of the summation of the energy dissipated by the bottom floor fuses divided by the total energy dissipated by all fuses. In this loading sequence, the lower floor fuses dissipate approximately 30% more energy than the upper floor fuses.

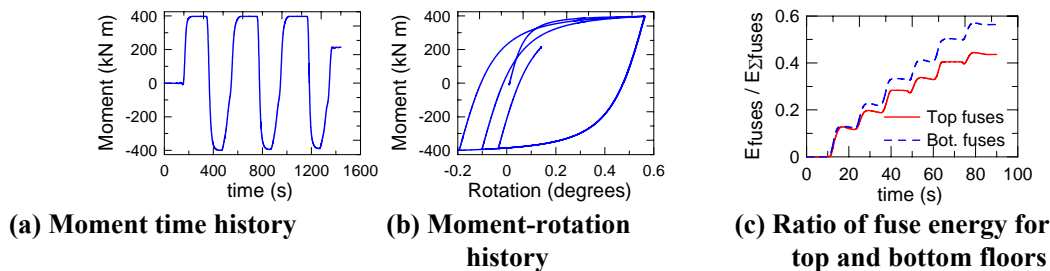


Figure 5. Two bay fuse results: test HSC 16 (prototype units).

Acceleration Distribution

The accelerometers placed in the soil and on the structure can be used to estimate the period of the site and the distribution of acceleration amplification within the structure. In estimating the site period, one

may compare with theoretical estimates. Dry dense sand ($D_r=80\%$) has a shear wave velocity of approximately 80 to 110 m/s (using an estimated shear modulus G of 13270 to 19030 kPa from Das, 2004), which results in a characteristic site period of 0.14 to 0.20 seconds (estimated as $T=4H/V_s$). In observing the peak of ratios of the spectra from the measured soil accelerations, the site period is estimated as 0.2 seconds, which is in agreement with theoretical estimates.

Comparison with the acceleration signals recorded at the first and second floors of the structural model shows that the magnitude of the input acceleration signal increases as it travels up the structure, as is expected. Figure 6 shows the ratio of the peak structural accelerations measured at different points along the structures height, normalized by the peak input acceleration from an accelerometer at mid-height of soil layer. This ratio is defined as an amplification ratio Ω and plotted versus the height of the structure, normalized by the total height. These data show nearly a first mode linear response, with an approximate amplification of two at the upper floor level. Note that the large initial data points near to the ground surface are due to the normalization of peak structural acceleration by an accelerometer at mid-height of the soil layer. Accelerometers were not placed at the ground surface due to instrument count limitations. It is notable that the one and two bay amplification distribution is quite similar. Additionally, it is important to observe the change in slope of Ω at approximately mid-height due to the location of the first floor beam-column joints.

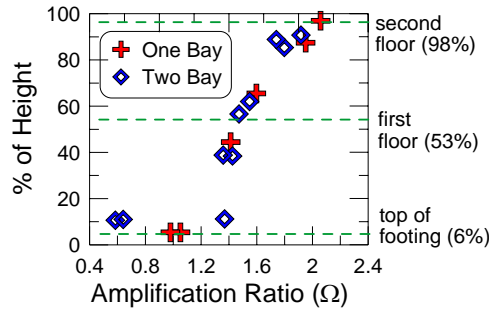


Figure 6. Acceleration Amplification Ratio Ω for tests D3 and D7.

Footing Response

Footing response is characterized by the moment-rotation, shear sliding, and axial force-settlement histories. Sample data from tests D3 and D7 for the one and two bay models, respectively, are shown in Figures 7 and 8. Note that these data are not shown beginning with zero moment or rotation, due to the cumulative load and deformation from the previous test series. Footing response for the one bay test D3 (Figure 7), shows that energy dissipation is occurring for the strip and square footings, largely in the form of moment-rotation for the strip footing and shear-sliding for the square footing. The asymmetry of the one bay structure is again observed at the footing level by the large amount of permanent rotation that the column

undergoes (approximately 1.6°). Permanent sliding of the column (square footing) is also greater than that for the shear wall (strip footing); as is the vertical settlement at this point in the testing chronology. In addition, the stiffer wall direction (as opposed to the column direction) can be observed in both the moment-rotation and shear-sliding response by observing the slope of the force-displacement response during loading in each of these directions. Approximately 80 mm of permanent settlement is cumulated for both the strip and square footings during this loading chronology. The rapidly degrading moment during increasing rotational demands at both the footings may be attributed to local bearing failure below the footings occurring during increasing reversed cyclic loading. Note that the rotational stiffness for the strip footing averages from 7000 kNm/rad to 6400 kNm/rad from 0 to 0.2 degrees, then degrades rapidly as the wall is loaded to 0.4 degrees. In contrast, the rotational stiffness of the square footing remains fairly stable; however, moment demand at the square footing reduces with increased cyclic rotational demand. This may be attributed to the reduced force demand within the structure as the beam-column joints continue to cumulate plastic demands, which occur above the column footing.

Examination of the footing response for test D7 (Figure 8) shows energy dissipation occurring in the strip and square footings. For the two bay model during test D7, the strip footing dissipates 88% of the total moment-rotation energy. The footing response for the two bay model reveals slightly different response as compared to that of the one bay model.

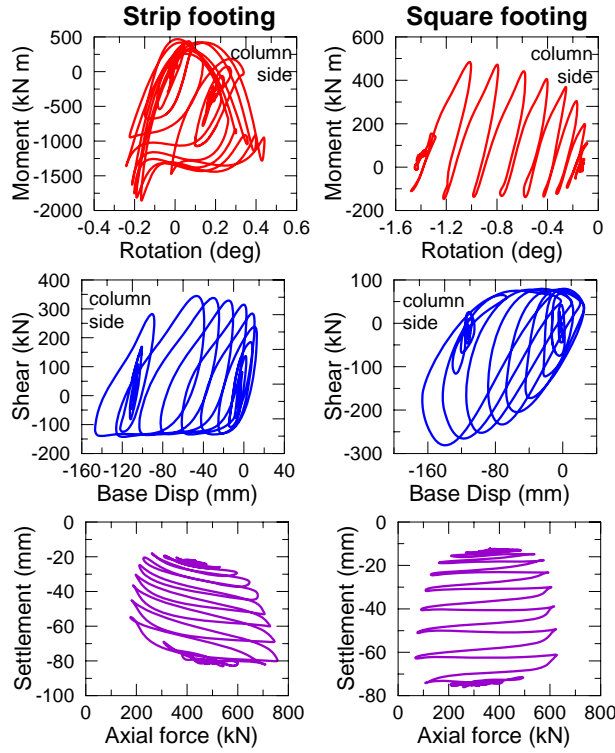


Figure 7. Response of footings during Test D3.

The degradation in rotational stiffness for the footings is not as significant for this loading sequence. However, for the exterior square footing, a stiffening of the footing is observed as the model reaches approximately 0.6 degrees -- likely due to the closing of a gap around the footing. Gapping surrounding the ends of each footing was observed during post-test physical inspection (Figure 9).

Later in the testing sequence, for example in test HSC 15 (not shown due to space limitations), compaction of the soil beneath the strip footing appears to have reached a limit. Although increasing axial force produces downward vertical displacement of the strip footing, a decrease of this same axial force releases this same strip footing and allows it to move upwards again. The shear versus sliding response for the strip footing is similar to that of the previously mentioned one bay model. However, significant stiffness changes are observed in the two bay model for both the interior and

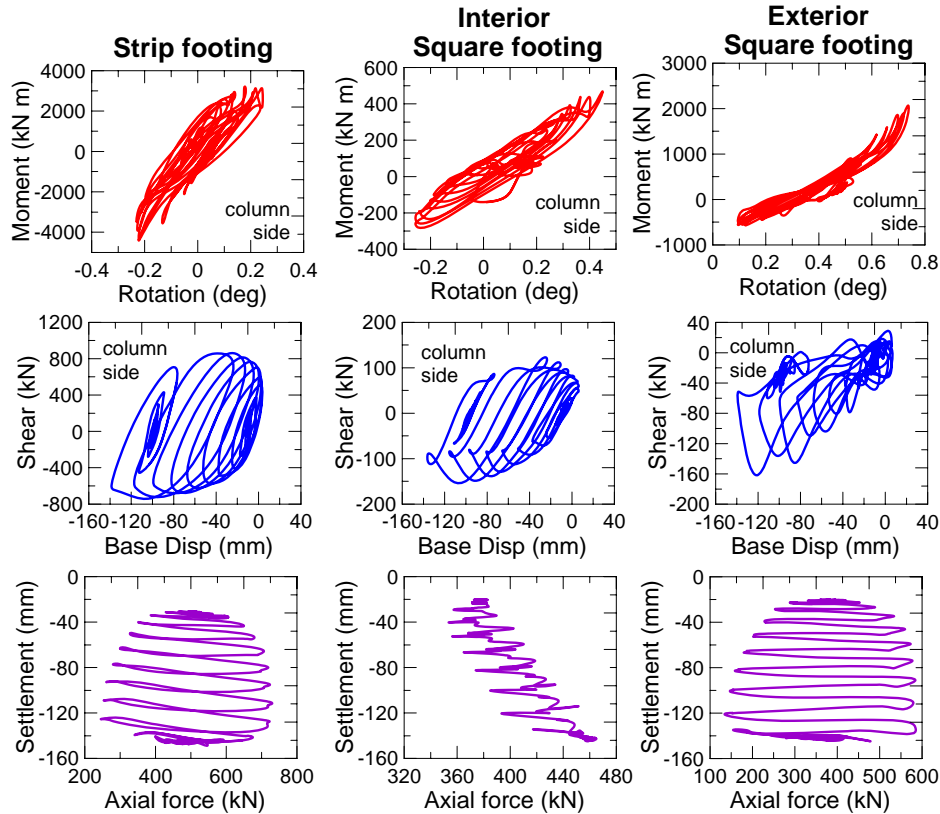


Figure 8. Response of footings during Test D7.

exterior footings -- also likely due to the gapping developed during repeated cyclic loading (Figure 9).

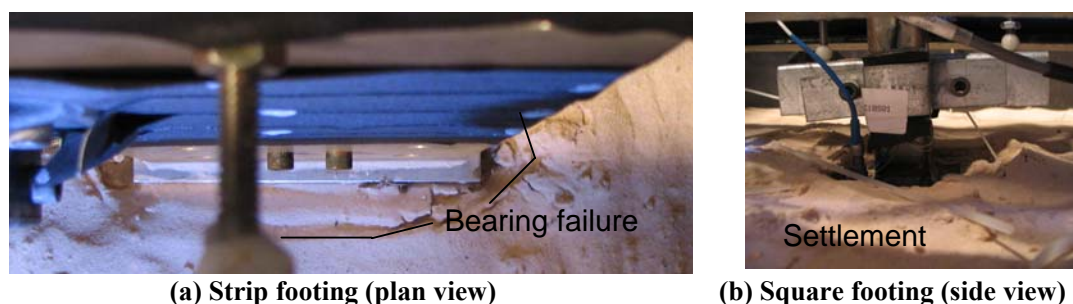


Figure 9. Photos of observed bearing failure and accrued settlement at strip and square footings after test HSC 8.

The moment capacities of the strip and exterior square footing are greater than the moment capacities from isolated footings tests at constant axial load (from previous experiments SSG03 and JMT01; the square footing capacity = 0.325 MN-m; strip footing capacity = 0.700 MN-m). Inspection of the previous plots shows redistribution of the vertical loads as the structure rocks; this changing vertical load will affect the moment capacity. Increased moment capacity is associated with momentary large axial load on the footing.

Energy Dissipation of the Footings

Energy is dissipated in both models through nonlinear actions at both the footing and beam-column joints. The amplitude of this energy is calculated by summing the area under either the moment-rotation, shear-sliding, or axial-settlement responses. Examination of the relative amounts of dissipated energy by the strip and square footings shows that much more energy is initially dissipated through the moment-rotation action of the strip footing in the one bay model tests (Figure 10). These bar charts separately indicate the moment versus rotation and shear force versus base sliding energy dissipation of the one bay footings. At the beginning of the test chronology, the energy dissipated through moment-rotation behavior of the strip footing often reaches 90% of the total moment-rotation energy. In contrast, the strip and square footing tend to approximately equally contribute to the shear-sliding energy dissipation; though it should be noted that at low amplitude loading, the footing is likely not yielding in either (or all of) moment, shear, or axial modes. Though not shown, it is observed that axial force-settlement behavior shows a larger contribution coming from the strip footing. For a heavily asymmetric structure, such as the one bay model, the energy dissipated by the wall strip footing is much more significant than that of the column footing.

The two bay model also indicates that the strip footing tends to dissipate more moment-rotation energy than the column footing, particularly as compaction of the soil increases (Figure 11). Among the three footings, the strip footing can dissipate up to 80% of the total moment-rotation based footing energy. During particular two bay tests where little horizontal sliding occurs (HSC 11 and HSC 13), the middle square footing also provides a significant contribution to energy dissipation through moment action because the two bay structure tends to rock about the middle square footing. In contrast, the exterior square footing dissipates less comparative energy as the soil compacts. For the first two loadings, the exterior square footing contribution is comparatively larger than the strip footing contribution because the strip footing has not yielded yet. Similarly, as the soil compacts, the exterior square footing contributes decreasing comparative energy for shear-sliding dissipation; meanwhile the interior square footing and the strip footing are both making significant contributions.

Comparing overall amounts of energy dissipated by the moment-rotation, shear-sliding, and axial-settlement of the footings per test for the one bay model are shown in Figure 12. After initial settlement of the structure occurs and the soil compacts, the amount of energy dissipated by axial-settlement decreases. The shear-sliding and moment-rotation contributions then steadily increase until, by the last one bay loading series, the moment-rotation is approximately half of the overall energy

dissipated by the footings. Two bay tests show the same overall trend (Figure 12). In the early loading stages of testing, axial-settlement dissipates more energy than either moment-rotation or shear-sliding. As the soil compacts, the axial-settlement contribution decreases; however, moment-rotation and shear-sliding contributions continue to increase.

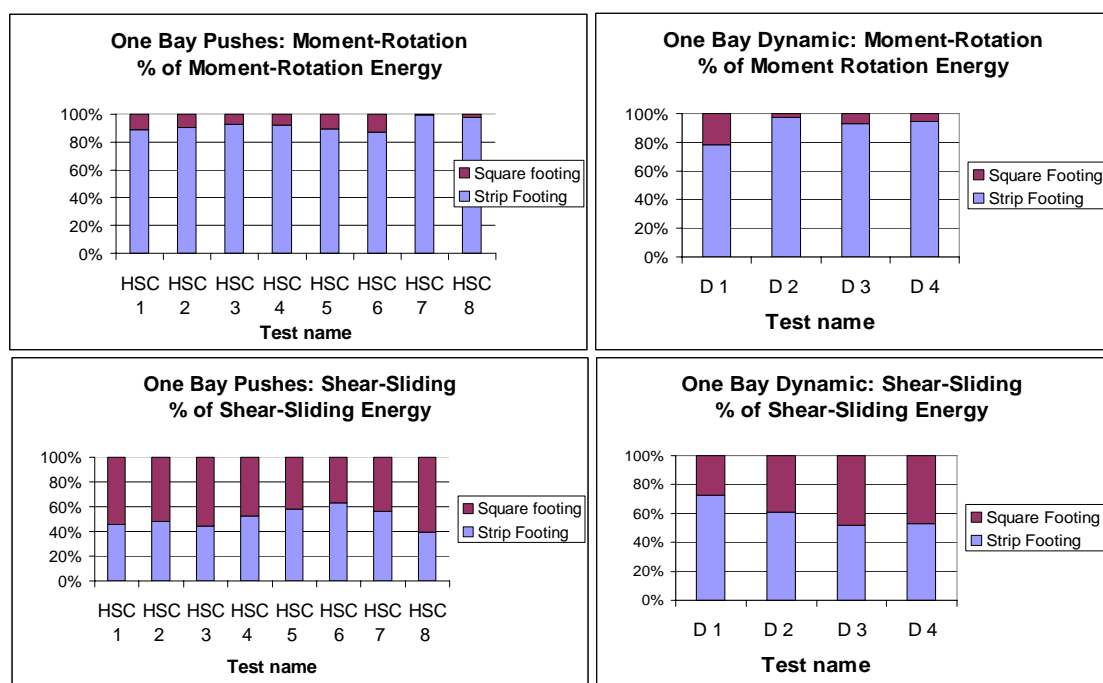


Figure 10. One Bay Tests: Individual footing energy

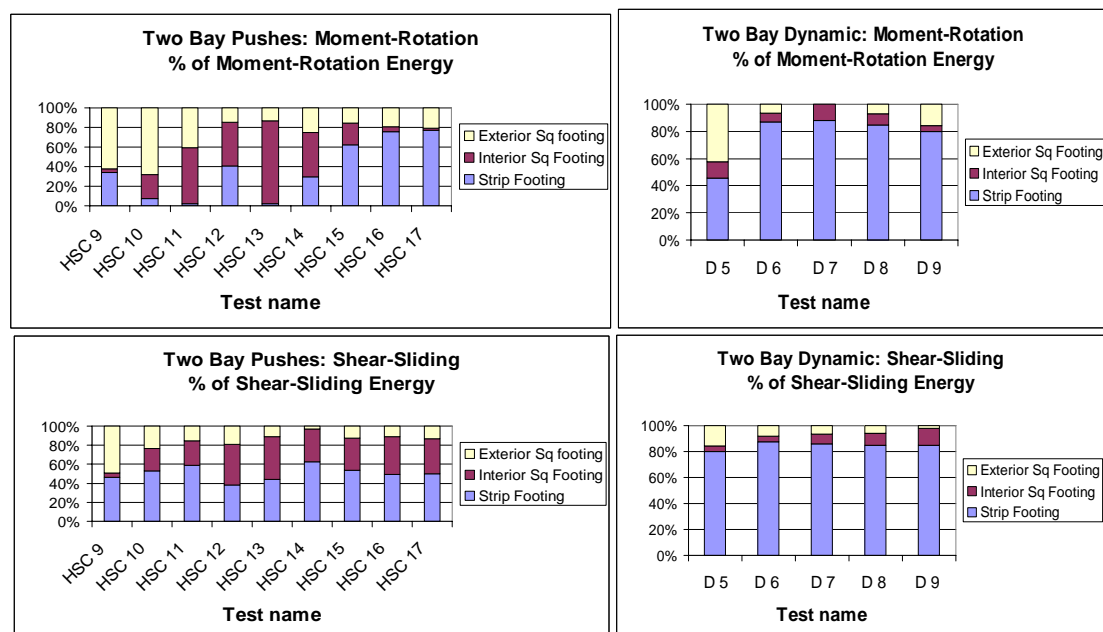


Figure 11. Two Bay Tests: Individual footing energy

If the energy dissipated by the beam-column fuses and the footings are compared (Figure 13), it is observed that at low drift ratios, nearly all of the total system energy is dissipated by the footings. This is consistent for both the one bay and the two bay model tests. As the maximum absolute drift demand on the model is increased, the portion of energy dissipated by the footings decreases, and the beam-

columns joints dissipate more of the total system energy. Contribution from the footings ranges from 65% to 80% of the total system energy as drift increases. With increasing structural drift comes an increasing percentage of energy dissipated by the beam-column joints.

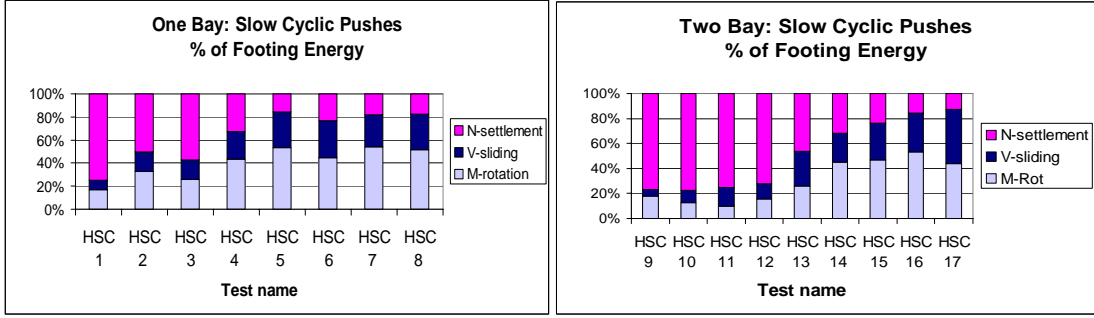


Figure 12. Summary footing energy by distribution of moment, shear, and axial modes.

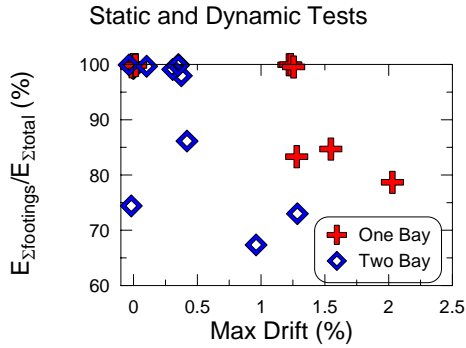


Figure 13. Fraction of energy dissipated by the footings

CONCLUSIONS

In this paper, which focuses on combined soil-structure systems, the effectiveness of the commonly adopted retrofit strategy of adding a shear wall to a reinforced concrete frame is studied through centrifuge testing. Two 20g model frame-wall-foundation structures supported on strip and square footings and embedded in dry dense Nevada sand were tested on the UC Davis centrifuge. Loading sequences included dynamic base excitation and slow cyclic inertial-based input. Data analysis of the centrifuge experiments indicates that these frame-wall systems have highly asymmetric hysteretic

loops due to the asymmetry of the lateral force resisting system; in this case, the shear wall is in an unsymmetrical position on one end of the building. For footings with a fairly large factor of safety against collapse due to vertical loads, the moment capacity of the footing increases as the vertical load on the footing increases. Thus footings at the edge of the building that are subject to cyclic axial load will behave differently than these footings near the center of the frame, where axial loads may be more constant. It is also observed that significant system-level energy dissipation occurs in the model during both pseudo-static and dynamic loading. This occurs due to both footing and beam-column fuse nonlinear action. Although moment-rotation energy provides an important contribution to all footing energy dissipated, compaction of the soil underneath the footings also affects which footing mechanism contributes most to the energy dissipated by the footings. At low drift ratios, more than 90% of the total system energy is dissipated by the footings. As drift demand increases, the contribution of energy dissipated by the footing decreases. For this system, at drift ratios up to approximately 2%, at least 65% of the total energy dissipated by the system is coming from the footings through the combined actions of moment, shear, and axial modes -- with the largest fraction generally through moment-rotation action.

The centrifuge tests reported here are among the first model scale experiments that have included reasonably accurate simulations of building nonlinearity coupled with foundation nonlinearity. It is envisioned that this work will fill a critical gap in characterizing the system level ductility of dual lateral resisting systems, where soil structure interaction is considered.

ACKNOWLEDGEMENTS

This work was supported by the Pacific Earthquake Engineering Research Centers program of the National Science Foundation under award EEC-9701568, PEER project number 1092004a. The helpful suggestions and support of Professor Geoff Martin, Craig Comartin, and Mark Moore are greatly appreciated. We also acknowledge the professional support provided by staff of the Center for Geotechnical Modeling at UC Davis that made this work possible. Any opinions, findings, and conclusions expressed in this paper are those of the authors, and do not necessarily reflect those of the sponsoring organization.

REFERENCES

- ACI 318-02, 2002, Building Code Requirements for Structural Concrete (ACI 318-02) and Commentary (ACI 318R-02), American Concrete Institute, Farmington Hills, MI
- Barlett, P. E., 1976, Foundation Rocking on a Clay Soil, *M.E. Thesis*, University of Auckland, New Zealand
- Chang, B. and Thomas, J. and Gajan, S. and Kutter, B. and Raychowdhury, P. and Hutchinson, T. 2006a, Centrifuge Data Report for JMT02 Test Series, Center of Geotechnical Modeling Data Report (*In preparation*).
- Chang, B. and Raychowdhury, P. and Hutchinson, T. and Thomas, J. and Gajan, S. and Kutter, B., 2006b, Centrifuge Testing of Combined Frame-Wall-Foundation Structural Systems (Paper #998), *8th U.S. National Conference on Earthquake Engineering by EERI, April 18-22, 2006*.
- Das, Braja M., 2004, *Principles of Foundation Engineering*, 5th ed, Brooks/Cole-Thomson Learning
- FEMA 356, 2000, Prestandard and Commentary for the Seismic Rehabilitation of Buildings, American Society of Engineers, Virginia
- Gajan, S. and Phalen, J. and Kutter, B., 2003, Soil-Foundation Structure Interaction: Shallow Foundations: Centrifuge Data Report for the SSG02 and SSG03 Test Series, Center for Geotechnical Modeling Data Report UCD/CGMDR-03/01 and Data Report UCD/CGMDR-03/02
- Gajan, S., Kutter, B. L., and Thomas, J. M., 2005, Physical and Numerical Modeling of Cyclic Moment Rotation Behavior of Shallow Foundations, *16th International Conference on Soil Mechanics and Geotechnical Engineering*
- Harden, C., 2003, Numerical Modeling of the Nonlinear Cyclic Response of Shallow Foundations, *Master's Thesis*, University of California, Irvine
- Housner, G.W., 1963, The Behavior of Inverted Rocking Pendulum Structures during Earthquakes, *Bulletin of the Seismological Society of America* 53 (2), 403-417
- Kutter, B., 1997, Dynamic Centrifuge Modeling of Geotechnical Structures, *Transportation Research Record 1336*, University of California, Davis
- Mander, J.B. and Priestley M.J.N. and Park, R., 1988, Theoretical Stress-Strain Model for Confined Concrete, *Journal of Structural Engineering*, (ASCE) Vol. 114, No. 8, August 1988
- Negro, P. and Verzeletti, G. and Molina, J. and Pedretti, S. and Lo Presti, D. and Pedroni, S., 1998, Large-Scale Geotechnical Experiments On Soil-Foundation Interaction: (TRISEE Task 3), *European Commission, Joint Research Center, Special Publication*, No. 1
- OpenSEES, 2006, Open System for Earthquake Engineering Simulation PEER (opensees.berkeley.edu)
- Rosebrook, K. R. and Kutter, B. L., 2001, Soil-Foundation Structure Interaction: Shallow Foundations, Centrifuge Data Report for the KRR01, KRR02, KRR03 Test Series, Center for Geotechnical Modeling Data Report UCD/CGMDR-01/09, UCD/CGMDR-01/10, UCD/CGMDR-01/11
- Wiessing, P. R., 1979, Foundation Rocking on Sand, *School of Engineering Report No. 203*, University of Auckland, New Zealand